

# Dynamics of Directional Drift in Brownian Motion of Molecules with Broken Symmetry in Dilute Solutions

Nan Sheng<sup>1</sup>, YuSong Tu<sup>2</sup>, Pan Guo<sup>1</sup>, RongZheng Wan<sup>1</sup>, ZuoWei Wang<sup>3,†</sup>, and HaiPing Fang<sup>1,\*</sup>

<sup>1</sup> *Division of Interfacial Water and Key Laboratory of Interfacial Physics and Technology, Shanghai Institute of Applied Physics, Chinese Academy of Sciences, P.O. Box 800-204, Shanghai 201800, China*

<sup>2</sup> *College of Physics Science and Technology, Yangzhou University, Jiangsu, 225009, China*

<sup>3</sup> *School of Mathematical and Physical Sciences, University of Reading, Whiteknights, Reading RG6 6AX, United Kingdom*

## Abstract

**We show by three-dimensional molecular dynamics simulations that the Brownian motion of molecules/particles with broken symmetry in very dilute solutions includes a directional drifting process. The time-dependent probability distribution function of the center of mass position of such a particle shows a bias towards its original orientation direction at short time scales, leading to a non-zero directional mean displacement whose value saturates as the rotational autocorrelation function of the particle decays completely. For model particles shaped as triangular pyramids, the saturated value of the drift is found to grow almost linearly with the particle size. Our detailed force analysis reveals that the physical origin of the drifting behavior arises from the imbalanced forces acting on the model particles by surrounding solvent molecules, which generate an effective net force pointing to the original orientation direction. The directional motion of the particle takes place in the crossover region from ballistic to diffusive motion, which is a pre-diffusive behavior beyond the scope of conventional diffusion theories using Einstein relationship. A phenomenological model description of the drifting behavior has been proposed based on the coupling with rotational relaxation. Our simulation and theoretical finding thus provide novel insights into the fundamentals of particle**

**diffusion and the understanding of various physical, chemical and biological processes that usually happen in nanoscale space within a finite time.**

## **Introduction**

Diffusion is one of the most fundamental processes in nature. As a basic type of movements in cells of life, diffusion is strongly associated not only with the transfer of materials, such as water<sup>1-3</sup>, proteins<sup>4-6</sup> and nucleic acids (e.g., DNA<sup>7,8</sup>), but also with the interactions between these molecules and their immediate environment to achieve biological functions.<sup>9</sup> Diffusion is also extensively involved in kinetic processes, such as molecular/particle dispersion<sup>10-13</sup>, aggregation<sup>13-17</sup> and chemical reaction<sup>18,19</sup>.

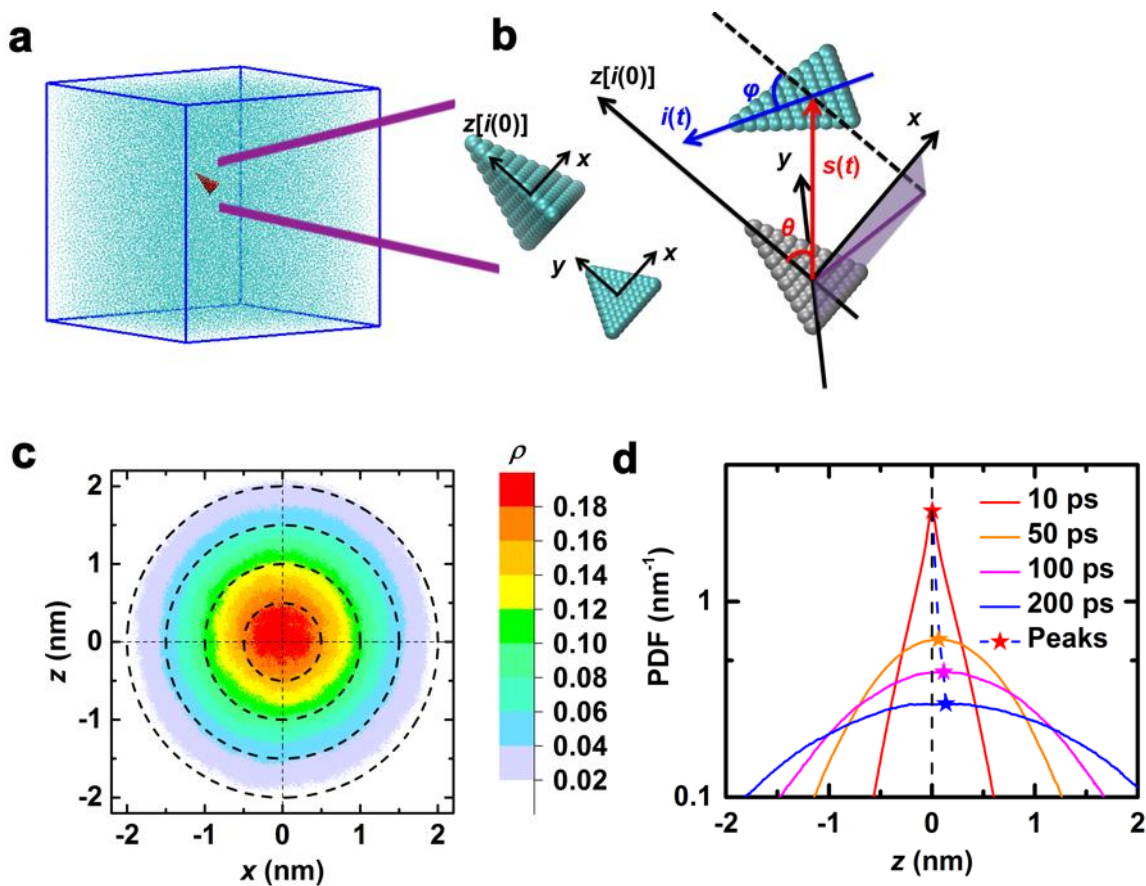
In conventional theory, the diffusing molecule/particle is simply assumed as a perfect sphere whose trajectory can be described as a random walk and the mean square displacement (MSD) obeys the Einstein relationship.<sup>20</sup> However, most of the molecules and particles have intrinsically specific structures, which are clearly different from spheres. Their diffusion behavior will surely be affected by the molecular architectures and are not necessarily isotropic any more. For example, Han et al. observed the anisotropic diffusion of ellipsoidal particles along different axial directions within timescales up to second,<sup>21</sup> although the trajectory of such particles returns to be isotropic if the interval between two sequential sampling records is at large enough timescales, i.e., more than 1 minute. Since an ellipsoidal particle has central symmetry about its center of mass (CoM), the diffusions in the two opposite directions along any given line passing through its CoM are equivalent. Similarly, macromolecules with symmetric structures such as linear polymer chains and DNAs also diffuse symmetrically along the chain axes without net movement of the centers of mass.

However, many real molecules/particles, such as water and ethanol, possess geometrically asymmetric structures. For example, water molecule has a triangular geometry, where the two

hydrogen heads are clearly different from the rear oxygen atom. Thus, they are expected to display anisotropic diffusion behavior. Theoretical works on the diffusion of anisotropic particles have been mainly contributed to describe the coupling between the translational and rotational movements and the resulted diffusion coefficients.<sup>22-25</sup> In a previous work based on molecular dynamics (MD) simulations, we observed that the Brownian motion of some small asymmetric solute molecules, such as methanol and glycine, have preference in certain specific directions along with the orientations of the molecules, indicating that there are directional drifting processes.<sup>26,27</sup> Chakrabarty et al. found experimentally that the Brownian motion of boomerang colloidal particles of micrometer size confined in two-dimensions (2D) exhibits a biased mean displacement towards the center of hydrodynamic stress (CoH), if the cross point of the two arms, which represents the center of body (CoB), is chosen as the point for motion tracking.<sup>28,29</sup> This also implies the existence of a directional motion of the CoM, though not explicitly addressed in that work. The experimental observation was interpreted using an analytical model based on Langevin theory as the result of nonoverlap between the CoH of the boomerang particle and the tracking point (CoB).

In this work we tackle the problem by investigating the Brownian motion of model particles shaped as triangular pyramids in very dilute solutions using both three-dimensional (3D) molecular dynamics simulations and theoretical analyses. Our MD simulations with explicit solvents are carried out by solving dynamic equations based on direct interactions among particles, and so avoid making any prior assumptions, such as isotropic random fluctuations and isotropic dissipation, as used in the Langevin equation. We find that the non-zero effective driving force for such directional motion results from the imbalance of the frictional forces experienced by the constituent atoms of the model particles during the orientation regulation. Thus, the directional drift is well correlated with the rotational autocorrelation functions of the asymmetric particles. When the rotational autocorrelation function decays completely, the accumulation of the directional drift saturates at a value that is almost linearly proportional to the size of the particle. The saturated value of the drift or mean displacement

cannot be ignored in comparison with the diffusion distance of the particle within finite time. We note that extensive physical<sup>30-32</sup>, chemical<sup>33</sup> and even biological processes<sup>5,34</sup>, including protein conformation changes<sup>35,36</sup>, occur in a finite time, e.g., nano-, pico- and even femto-seconds. Therefore, our finding may contribute to understanding the microscopic mechanisms of various kinetic processes and their practical applications, such as chemical separation<sup>37</sup>, sensing<sup>38-40</sup> and drug delivery<sup>41,42</sup>, especially at short timescales. Furthermore, it extends the understanding of fundamental diffusive processes to nano-world beyond the conventional theory of Einstein diffusion relationship.



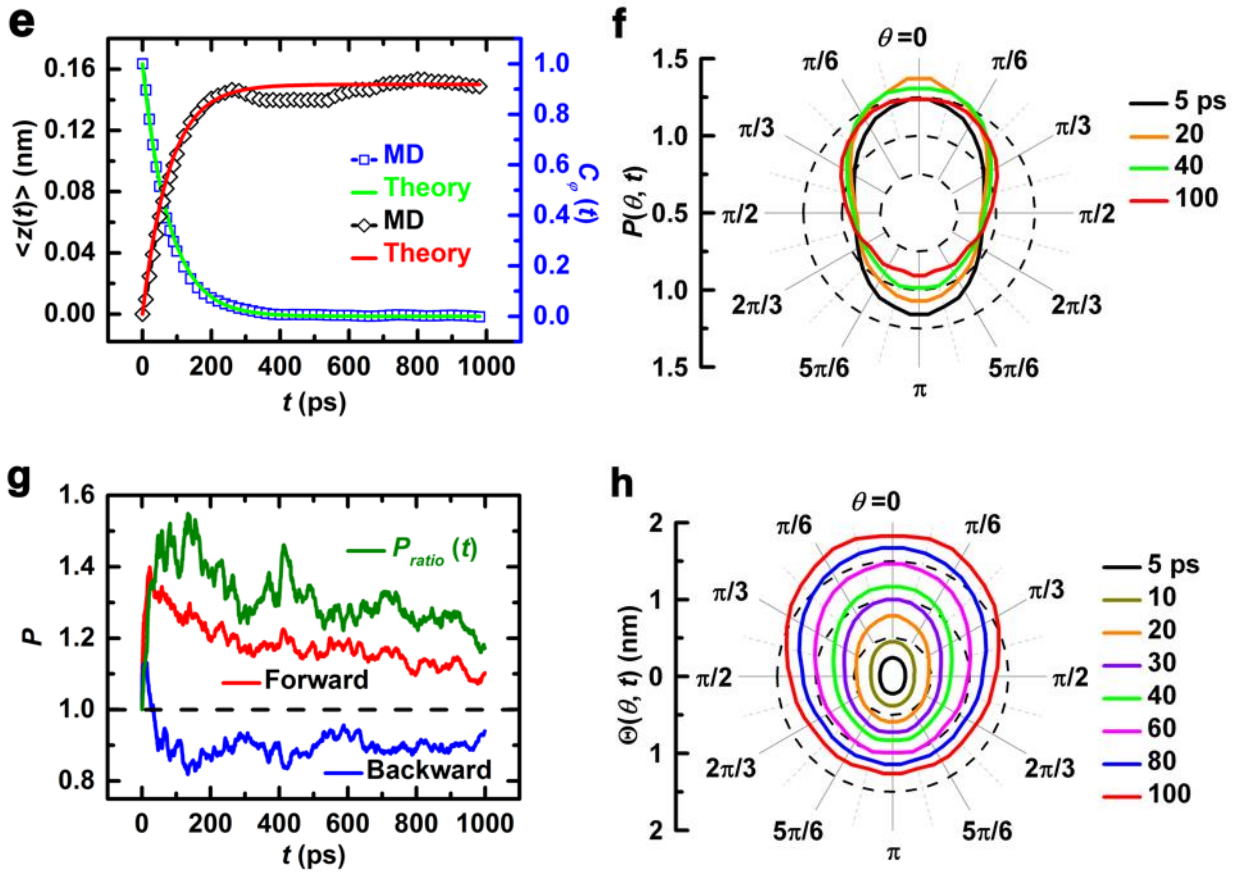


**Figure 1** (a) Snapshot of the simulation system consisting of a model particle shaped as a triangular pyramid with height  $h = 1.68$  nm (as shown next to the box) in dilute solution. The cyan points represent the solvent particles and the asymmetrical model particle is red highlighted. (b) A 3D Cartesian coordinate frame defined for a target model particle with the origin point fixed at the initial location of its center of mass and the  $z$ -axis aligned along its initial orientation  $\mathbf{i}(0)$  at time  $t = 0$ . The other two axes are set on the triangular base of the particle. The orientation of the particle at time  $t$ ,  $\mathbf{i}(t)$ , is defined by the unit vector pointing from the center of the triangular bottom to the top of the pyramid. The displacement of the particle at time  $t$  is the vector  $\mathbf{s}(t)$ . The position angle  $\theta$  is between  $\mathbf{s}(t)$  and the  $z$ -axis  $[\mathbf{i}(0)]$ , and the orientation angle  $\varphi$  is between  $\mathbf{i}(t)$  and the  $z$ -axis. (c) Probability density function (PDF) of the CoM position at  $t = 100$  ps projected onto the  $xz$ -plane, where different colors stand for different probability densities,  $\rho$ , and black dashed circles are included for guiding the eyes. (d) Probability density function of the CoM position projected onto the  $z$ -axis at different time  $t$ , where the stars mark the peaks of the PDFs. (e)  $z$ -component of the mean position of the particle CoM with respect to time (open black diamonds). The red line is the theoretical curve of  $A[1-C_\phi(t)]$  [Eq.(18)]

with  $A = 0.15$  nm. The open blue squares are the autocorrelation function of the particle orientation  $C_\phi(t)$  obtained from MD simulation. The green curve represents an exponential relaxation function  $\exp(-2D_r t)$  with the rotational diffusion coefficient  $D_r = 6.48 \times 10^{-3}$  rad<sup>2</sup> ps<sup>-1</sup> [see Eq.(2) and SI]. (f) Relative deviation of probability  $P(\theta, t)$  of the particle displacements with respect to the position angle  $\theta$  at time  $t$ , as defined in Eq. (5). The value of  $P = 1$  corresponds to the case of isotropic diffusion. The dashed circular curves are included for guiding the eyes. (g) Relative deviations of probability for the particle diffusing within  $10^\circ$  away from the  $z$ -axis in the positive [ $P(0, t)$ , Forward, red line] and the opposite [ $P(\pi, t)$ , Backward, blue line] directions as a function of time.  $P_{ratio}(t)$  (green line) is the ratio of  $P(0, t)$  over  $P(\pi, t)$ , which is Eq. (6). (h) Mean accumulated displacements  $\Theta(\theta, t)$  of the particle in various directions for different time intervals (colored circles). The dotted circular curves are included for guiding the eyes.

## Results from MD simulations

Our simulation system consists of a single model particle shaped as triangular pyramid dispersed in a solvent of small Lennard-Jones particles with periodic boundary conditions applied in all three directions, as shown in Fig. 1(a) and described in the Simulation Method section. The MD simulation algorithms we employed have been widely used in the study of dynamics of molecules at nanoscale.<sup>43-53</sup> As detailed in SI, the size of the simulation box is large enough to make finite size effect<sup>54-56</sup> negligible. The 3D Cartesian coordinate frame used for the particle motion analysis is demonstrated in Figure 1(b) where the origin point and  $z$ -axis are built based on the initial location of the CoM and orientation  $\mathbf{i}(0)$  of the asymmetric model particle at a given reference time  $t = 0$ . Just like the calculation of any time correlation functions, each MD simulation time step can be taken as a time origin. All simulation results presented in this work are ensemble-averaged values obtained by using time origins separated by 1ps along the MD trajectory after the MD system has reached equilibrium state, see Simulation Method. Figures 1(c-h) show the simulation data for the model particle with height  $h = 1.68$  nm. The probability density function (PDF) of the CoM position of the particle at time

$t = 100$  ps projected on the  $x$ - $z$  plane is shown in Fig. 1(c). We note that there is a drift of the PDF toward the positive direction of the  $z$ -axis. Similar behavior is found in the PDF projected on the  $y$ - $z$  plane, but not on the  $x$ - $y$  plane (see SI). This drifting behavior can be seen more quantitatively in Figure 1(d) where the peak position of the PDF projected on the  $z$ -axis shifts toward the positive  $z$ -direction as time increases. On the contrary there is no directional shift of the PDF projections on the  $x$ - and  $y$ -axis. In Figure 1(d) the probability density function obtained at  $t = 10$  ps can be well described by an exponential function,  $\exp(-|x-\mu|/\delta)$ , where  $\mu$  is the mean value and  $\delta$  is the deviation, while the PDF at longer time, such as  $t = 200$  ps approaches to the form of Gaussian distribution,  $\exp(-(x-\mu)^2/\sigma^2)$ . This reflects the transition from the ballistic motion to classic diffusion (discussed in SI).

We also calculate the mean position or displacement of the CoM of the model particle on the  $z$ -axis [Fig. 1(e)] as a function of time,

$$\langle z(t) \rangle = \langle \mathbf{s}(t) \cdot \mathbf{i}(0) \rangle = \langle |\mathbf{s}(t)| \cos \theta \rangle, \quad (1)$$

where  $\theta$  is the angle between the displacement vector  $\mathbf{s}(t)$  and the initial orientation ( $z$ -axis) of the particle as defined in Fig.1(b). The results on  $\langle x(t) \rangle$  and  $\langle y(t) \rangle$  are given in SI. Only along the  $z$ -axis, the mean displacement shows a significant growth with time. As shown in Fig. 1(e),  $\langle z(t) \rangle$  increases rapidly when  $t < 100$  ps and gradually reaches a plateau value (0.15 nm) after 200 ps. This behavior is essentially different from the traditional theory on Brownian motion where the mean displacements of particles under no external influence are supposed to be zero, as already observed for spherical or ellipsoidal particles<sup>21</sup>. We have also computed the autocorrelation function of the particle orientation,  $C_\varphi(t)$ , which characterizes the particle rotational relaxation and is defined as

$$C_\varphi(t) = \langle \mathbf{i}(t) \cdot \mathbf{i}(0) \rangle = \langle \cos[\varphi(t)] \rangle = e^{-2D_r t}, \quad (2)$$

where  $\varphi(t)$  is the angle between the unit vectors  $\mathbf{i}(t)$  and  $\mathbf{i}(0)$  representing the particle orientations at time  $t$  and time zero. Conventionally,  $C_\varphi(t)$  is supposed to decay exponentially and the rotational diffusion coefficient  $D_r$  ( $= 6.48 \times 10^{-3} \text{ rad}^2 \text{ ps}^{-1}$ ) can be obtained by linearly fitting the mean square

angle of the particle orientation,  $\langle \varphi^2(t) \rangle$ , to the Einstein relation<sup>57</sup> (see SI). As shown in Fig. 1(e), apart from the very first dozens of picoseconds where the inertial effect dominates (more details in SI), the theoretical prediction of  $C_\varphi(t)$  agrees with the MD data very well up to the timescale of 1 ns.  $C_\varphi(t)$  first decays rapidly within 100 ps and almost vanishes after 200 ps. Comparing the  $C_\varphi(t)$  and  $\langle z(t) \rangle$  data in Fig.1(e) reveals an intrinsic correlation between the rotational and translational motion, as discussed below.

Since the drift mainly takes place along the  $z$ -axis, we re-analyze the 3D PDF in the polar coordinates with respect to the displacement angle  $\theta$ . The relative deviation of probability away from the isotropic diffusion,  $P(\theta, t)$ , for the case that the particle displacement falling in the range of  $[\theta, \theta + \Delta\theta]$  after time  $t$  is computed as

$$P(\theta, t) = \frac{n(\theta)}{NG(\theta)} \quad (3)$$

with

$$G(\theta) = \frac{\int_{\theta}^{\theta+\Delta\theta} \sin \vartheta d\vartheta}{\int_0^\pi \sin \vartheta d\vartheta}, \quad (4)$$

where  $n(\theta)$  is the number of cases that the particle displacement falling in the range of  $[\theta, \theta + \Delta\theta]$ , and  $N$  is the total number of cases sampled in the simulations.  $G(\theta)$  is the spherical integral weight of the range  $[\theta, \theta + \Delta\theta]$ . Here, we take  $\Delta\theta = 10^\circ$ . Figure 1(f) shows that the relative deviation of probability  $P(\theta, t)$  at any angle  $\theta < 60^\circ$  is always larger than the value of  $P = 1$  corresponding to isotropic diffusion, while  $P(\theta, t)$  at  $\theta > 90^\circ$  keeps decreasing from time  $t = 5$  ps to 100 ps. It indicates that the particle prefers to move forward along its initial orientation. This can be seen more clearly in Fig. 1(g) which compares the relative deviations of probability for the particle to diffuse forward within  $10^\circ$  from the  $z$ -direction  $[P(0, t)]$  and backward in the opposite direction  $[P(\pi, t)]$ . The ratio between these two quantities is measured by  $P_{ratio}(t)$

$$P_{ratio}(t) = \frac{P(0,t)}{P(\pi,t)} = \frac{n(0)}{n(\pi)}. \quad (5)$$

The value of  $P_{ratio}(t)$  reaches a peak of 1.55 at  $t \approx 130$  ps and remains above 1.20 until 1 ns, meaning

that the probability for the model particle to diffuse forward can be more than 50% higher than that for it to diffuse backward and still be over 20% higher for a time period of over 1 ns.

The statistical mean displacement of the model particle, denoted by  $\Theta(\theta, t)$ , in the direction of  $\theta$  after time  $t$  is calculated in a similar way as for calculating  $P(\theta, t)$ ,

$$\Theta(\theta, t) = \frac{\sum_{\theta}^{\theta+\Delta\theta} |\mathbf{s}(t)|}{NG(\theta)}, \quad (6)$$

where  $\sum_{\theta}^{\theta+\Delta\theta} |\mathbf{s}(t)|$  is the sum of the magnitudes of displacement falling in the range  $[\theta, \theta + \Delta\theta]$ . The results on  $\Theta(\theta, t)$  are shown in Fig.1(h) as the distorted colored circles, which demonstrate a clear preference for the particle to diffuse towards the directions of  $\theta < 90^\circ$  over towards the directions of  $\theta > 90^\circ$  and this trend becomes even more evident as time increases. Taking  $t = 100$  ps for instance, the difference between  $\Theta(0, t)$  and  $\Theta(\pi, t)$  is about 0.6 nm.

### Physical origin of the directional motion

In order to understand the underlying physics of the directional motion of the model particle, we compute the ensemble-averaged force  $\langle F_z(t) \rangle$  acting on the particle along the  $z$ -axis by surrounding solvent molecules. The result for the model particle studied in Fig. 1 is shown in Fig. 2(a) as a function of time. It is clear that  $\langle F_z(t) \rangle$  does have a positive value at early times. More specifically this force first increases starting from time zero, reaches its maximal value at 2 ps and then decreases. It becomes negative at 12 ps, reaches the minimal value at 17 ps and then gradually approaches zero. As a direct consequence, the  $z$ -components of both the mean translational velocity,  $\langle v_z(t) \rangle$ , [Fig.2(b)] and the mean displacement,  $\langle z(t) \rangle$ , [Fig.1(e)] possess positive values for over 200 ps time.

Now we focus on the physical origin of the driving force for the directional motion. This can be done by analyzing the ensemble-averaged force  $\langle F_z^i(t) \rangle$  acting on every individual constituent atom of the model particle, where  $i$  is the serial number of the atom under investigation. Apparently  $\langle F_z^i(t) \rangle$  only results from the fluctuating forces owing to the collision with the surrounding solvent. We separate the contributions of these forces to  $\langle F_z^i(t) \rangle$  into two parts. The first part is independent of the velocity

of the model particle and so its constituent atoms, equivalent to the effect of liquid pressure felt by a stationary object. As expected the ensemble average of such effects summing over all the atoms is zero at the CoM of the particle, and therefore makes no contribution to the motion of the CoM. The other part is velocity-dependent and can be described in the form of the frictional force  $\langle f_z^i(t) \rangle$  given by the solvent against the motion of the atom. Following the Stoke's law, this force is considered to be linearly proportional to the mean velocity of the atom  $\langle v_z^i(t) \rangle$ ,

$$\langle f_z^i(t) \rangle = -\lambda^i \langle v_z^i(t) \rangle, \quad (7)$$

where  $\lambda^i$  is the frictional coefficient of the atom. We note that the  $\lambda^i$  values are different for atoms located at different sites of the particle structure, depending on how they are in contact with the solvent. In practice, the frictional coefficient of each atom can be estimated from the linear relation between the measured mean frictional force  $\langle f_z^i(t) \rangle$  and mean velocity  $\langle v_z^i(t) \rangle$  (details shown in SI). The mean velocity of the  $i$ th atom,  $\langle v_z^i(t) \rangle$ , can be written as

$$\langle v_z^i(t) \rangle = r_o^i(t) \frac{d}{dt} C_\varphi(t) + \langle v_z(t) \rangle, \quad (8)$$

where  $\langle v_z(t) \rangle$  is the mean velocity of the particle CoM along the  $z$ -direction. The first term on the right-hand side (rhs) of Eq. (8) results from the rigid-body rotation of the particle, where  $r_o^i$  is the projection of the atom position vector  $\mathbf{r}^i$ , pointing from the particle CoM to the center of the  $i$ th atom, on the particle orientation axis and can be obtained directly from the construction of the particle structure. Then the total force acting on the particle with  $N$  atoms is

$$\langle F_z(t) \rangle = \sum_{i=1}^N \langle f_z^i(t) \rangle = -mC_1 \langle v_z(t) \rangle + mC_2 Q(t) \quad (9)$$

with

$$C_1 = \frac{\sum_{i=1}^N \lambda^i}{m}, \quad C_2 = \frac{\sum_{i=1}^N \lambda^i r_o^i}{m} \quad \text{and} \quad Q(t) = -\frac{d}{dt} C_\varphi(t), \quad (10)$$

where  $m = Nm_{LJ}$  is the mass of the model particle and  $m_{LJ}$  is the mass of each constituent atom defined in the Simulation Method section. The first term on the rhs of Eq. (9) always resists the translational motion of the particle CoM. It is the second term that could potentially provide an effective force generating the drift along the  $z$ -direction (Details shown in SI). The sign of this term is only determined by  $C_2$ , because  $C_\varphi(t)$  always decays with time and so  $Q(t) \geq 0$ . It indicates that the key

reason for the non-zero net force  $\langle F_z(t) \rangle$  lies in the imbalance of the frictional forces ( $C_2 \neq 0$ ) acting on the constituent atoms during the particle orientation regulation. This can only happen for particles with asymmetric structures. If the geometric shape of the particle is symmetric, the frictional forces acting on all atoms are well balanced ( $C_2 = 0$ ) and no directional motion can be observed, see examples given in SI.

Introducing Eq. (9) into the Newton's second law,

$$\langle F_z(t) \rangle = m \frac{d}{dt} \langle v_z(t) \rangle, \quad (11)$$

and solving the differential equation, we can obtain the mean velocity  $\langle v_z(t) \rangle$ ,

$$\langle v_z(t) \rangle = C_2 R(t) e^{-C_1 t}, \quad (12)$$

with

$$R(t) = \int_0^t Q(\xi) e^{C_1 \xi} d\xi. \quad (13)$$

The mean force acting on the particle is thus

$$\langle F_z(t) \rangle = m C_2 [Q(t) - C_1 R(t) e^{-C_1 t}]. \quad (14)$$

This formula further clarifies that the mean force on the particle can be nonzero only when  $C_2 \neq 0$ .

It is rather tedious to compute  $C_1$  and  $C_2$  from estimating the frictional coefficients  $\lambda^i$  of all the atoms. For practical purpose, we estimate  $C_1$  and  $C_2$  from the best fitting of the simulation data on  $\langle F_z(t) \rangle$  and  $\langle v_z(t) \rangle$  to Eqs. (14) and (12). As shown in Fig. 2, these theoretical formulae provide good description of the simulation results. In SI we use a smaller model particle consisting of 10 atoms to demonstrate that the fitted  $C_1$  and  $C_2$  values are in very good agreement with those directly calculated using Eq. (10). Figure 2 shows that both  $\langle F_z(t) \rangle$  and  $\langle v_z(t) \rangle$  have a steep initial increase starting from zero values at  $t = 0$ . This is because the relaxation of the particle orientation, as measured by the autocorrelation function  $C_\phi(t)$ , does not follow the exponentially decaying behavior within a very limited time period close to  $t = 0$ , giving rise to an initial increase of  $Q(t)$  (see detailed analysis in SI). There is a notable positive peak of the mean force  $\langle F_z(t) \rangle$  at  $t \approx 2$  ps and consequently a peak value of

about  $1.5 \text{ m s}^{-1}$  in the mean velocity  $\langle v_z(t) \rangle$  at  $t \approx 10 \text{ ps}$ . It means that the particle experiences an effective force driving it move forward along the initial orientation direction at very early time. After about 20 ps, the mean force decays from the negative peak to zero, then behaves just like a normal frictional force. The directional net velocity also decays from its peak value but at a much slower rate. As a result, the saturated value of the drift distance is reached at  $t \approx 300 \text{ ps}$ . It is noted that the time scale for  $C_\phi(t)$  to start exponential decay and so the mean force to reach its peak value is close to the characteristic time  $\tau \approx mD/k_B T$ , where  $D$  is the translational diffusion coefficient of the particle, which marks the transition of the particle motion from the inertial regime to the diffusional regime.<sup>58</sup> This transition is further evidenced in the mean square displacement data by the crossover from the ballistic to diffusive motion behavior (see SI). It implies that the initial increase of  $Q(t)$  and so  $\langle F_z(t) \rangle$  is related to the inertial behavior of the asymmetric particle. The directional drift process of the model particle takes place in the crossover region from the ballistic to diffusive motion regime. This process should also be distinct from the simple ballistic motion, because they have completely different physical origins. The ballistic motion happens before the collision of the model particle with solvent molecules, while the drift is driven by the imbalanced forces acting on the particle by surrounding solvent molecules during its rotation which involve many collision events. In the ballistic motion picture, the initial translational velocity of the CoM of the particle can be in any direction. As a result, the resulted mean displacement of the particle is zero.

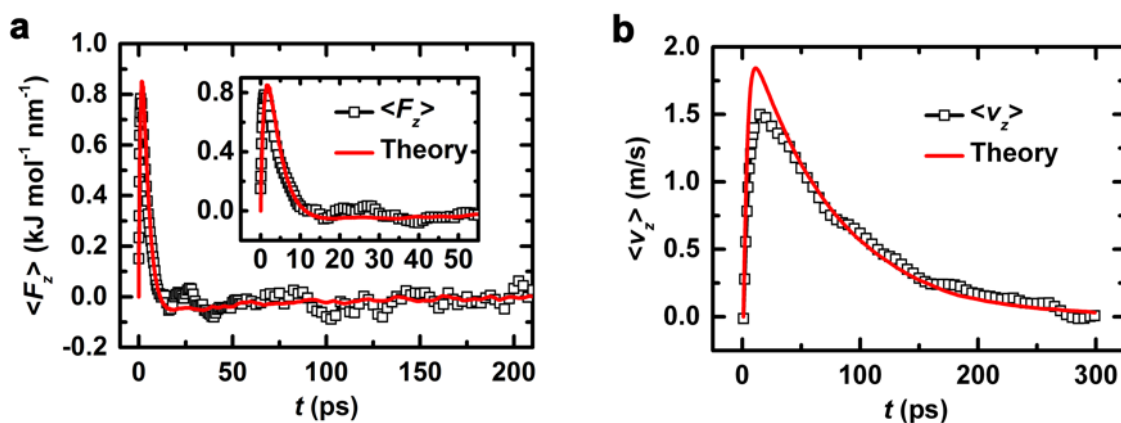


**Figure 2** (a) Mean force experienced by the model particle studied in Fig. 1 and (b) its mean velocity,

both along the  $z$ -axis. The solid curves are the best fitting of the simulation results (symbols) to the theoretical formulae in Eqs. (14) and (12), respectively.

### Theoretical description of the directional motion

The mean position  $\langle z(t) \rangle$  of the model particle can be obtained by integrating the mean velocity [Eq. (12)],

$$\langle z(t) \rangle = \int_0^t \langle v_z(\xi) \rangle d\xi = \frac{c_2}{c_1} [1 - C_\varphi(t) - R(t)e^{-c_1 t}]. \quad (15)$$

We notice that there is a saturation value of the drift,

$$A = \lim_{t \rightarrow \infty} \langle z(t) \rangle = \frac{c_2}{c_1}. \quad (16)$$

Equation (16) again suggests that the directional motion of the particle is only determined by  $C_2$ , which associates with the driving force. Since the term  $R(t)\exp(-C_1 t)$  has a peak height of only about  $0.02 \text{ s}^{-1}$  at  $t \approx 10 \text{ ps}$  and then decays rapidly to zero, we can simply write Eq. (16) at larger time scales ( $t > 10 \text{ ps}$ ) as

$$\langle z(t) \rangle \approx A[1 - C_\varphi(t)]. \quad (17)$$

Equation (17) clearly elucidates the simple correlation between  $C_\varphi(t)$  and  $\langle z(t) \rangle$ . It is shown in Figs. 1(e) and 5(b) that this expression provides very good description of the simulation data on  $\langle z(t) \rangle$ . We note that Charkrabarty et al. obtained a similar theoretical result as equation (17) for the relationship between the mean displacement of the tracking point and the particle rotational autocorrelation function, e.g., see Eqs. (15a,b) in Ref. [29]. But the correlation function they used takes a single exponential form, because the theoretical calculations were carried out in the free diffusion regime.

Since the mean displacement of the particle (first moment of the PDF of its position) along the  $z$ -axis is non-zero due to directional drift, i. e.,  $\langle z(t) \rangle \neq 0$ , we choose to study the second moment of the PDF, namely the variance  $\text{Var}[z(t)]$  of the particle displacement, rather than its MSD which conventionally assumes  $\langle z(t) \rangle = 0$ . Based on the observed translation-rotation coupling picture, this quantity can be described by an empirical expression,

$$\text{Var}[z(t)] \equiv \langle [z(t) - \langle z(t) \rangle]^2 \rangle = 2 \int_0^t S_z(\xi) d\xi, \quad (18)$$

where

$$S_z(t) = D_z(1 - e^{-t/\tau_z}) \text{ with } \tau_z = \frac{mD_z}{k_B T}. \quad (19)$$

As shown in Fig. 3, Equation (19) fits the data from MD simulation very well with the one-dimensional (1D) diffusion coefficient  $D_z = 4.12 \times 10^{-3} \text{ nm}^2 \text{ ps}^{-1}$  and the velocity relaxation time  $\tau_z = 4.36 \text{ ps}$ . Considering that  $\langle [z(t) - \langle z(t) \rangle]^2 \rangle = \langle [z(t)]^2 \rangle - [\langle z(t) \rangle]^2$  and the 1D mean square displacement  $\langle \Delta z^2(t) \rangle \equiv \langle [z(t) - z(0)]^2 \rangle = \langle [z(t)]^2 \rangle$  as the initial position of the particle  $z(0) = 0$  in the defined Cartesian coordinate, equation (18) can be justified in the two time limits. At very small time scales ( $t < \tau_z$ ), equation (19) is approximated by  $S_z(t) \approx D_z t / \tau_z$  and so  $\text{Var}[z(t)] \approx \langle v_T^2 \rangle t^2$  where  $v_T$  is the velocity of thermal motion based on the equipartition theorem,  $k_B T = m \langle v_T^2 \rangle$ . It follows that the MSD of the particle  $\langle \Delta z^2(t) \rangle \approx \langle v_T^2 \rangle t^2 + [\langle z(t) \rangle]^2$ , reflecting the ballistic motion behavior plus a drift. On the other hand, at large enough time scales,  $\text{Var}[z(t)] \approx 2D_z t$  and the MSD  $\langle \Delta z^2(t) \rangle \approx 2D_z t + [\langle z(t) \rangle]^2$ . Owing to the limited saturation value of the mean displacement  $\langle z(t) \rangle$ , the Einstein relationship,  $\langle \Delta z^2(t) \rangle \approx 2D_z t$ , is recovered at large time. We note that the results in Fig. 3 are consistent with the 3D MSD of the model particle calculated in the laboratory coordinate system as shown in Fig. S3.1 of SI.

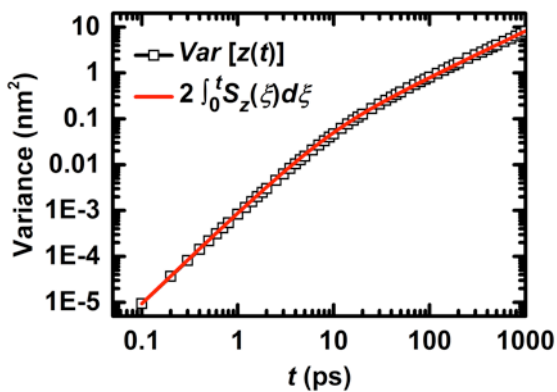
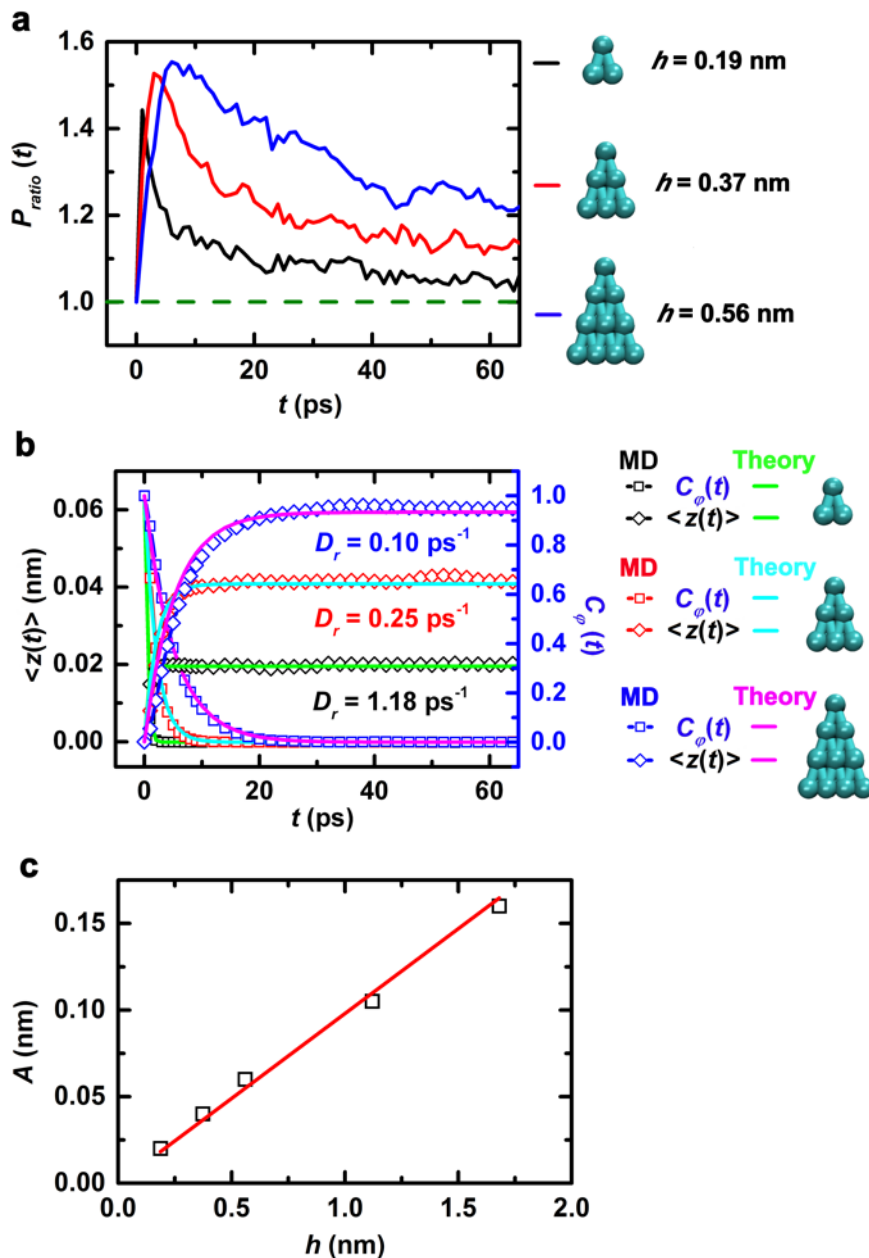


Figure 3. Variance of the displacement of the particle along the  $z$ -axis,  $\text{Var}[z(t)]$ , as a function of time. The solid red curve is the numerical fitting using Eqs. (18) and (19).

### Particle size dependence of the directional motion



**Figure 4** (a) Ratios,  $P_{ratio}(t)$ , between the probabilities for the model particles to move forward within  $10^\circ$  of their initial orientation directions and to move in the opposite direction. (b) Mean positions  $\langle z(t) \rangle$  along the  $z$ -axis and autocorrelation functions of orientation  $C_\phi(t)$  of the model particles of different sizes. The solid lines are theoretical predictions of Eqs. (2) and (17). (c) Saturated values  $A$  of the drift (black open squares) with respect to the heights of the model particles. The red line is a linear fitting of the simulation data to Eq. (24).

Figure 4(a) shows that the ratio of the probabilities for a model particle to move forward and

backward along its initial orientation direction decreases with the decrease of the size of the particle, indicating that the larger particles have more evident drifting behavior. Our theoretical expression [Eq. (17)] can describe the MD data on the time-dependent mean displacements very well for all the model particles studied [Fig. 4(b)]. Fig. 4(c) presents the saturated value  $A$  of the drift as a function of the particle size. Since all model particles have the same geometric shape, the projection of the atom position vector on the particle orientation axis has a simple linear relation to the height of the particle,

$$r_o^i \propto h. \quad (20)$$

It follows that the value of  $A$  is roughly linearly proportional to the size of the particle, given by substituting Eq. (20) into Eqs. (10) and (16),

$$A \approx kh, \quad (21)$$

where a constant value of  $k = 0.098$  is found by linear fitting to the simulation data in Fig. 3(c).

### **Potential detection and application of the directional drift**

The relatively small  $k$  value in Eq. (21) reflects that the magnitude of the directional drift is only a fraction (about 10%) of the model particle size. However, the impact of the drifting process can be detected at time and length scales much larger than the process itself. Figure 5 demonstrates one example of how the directional motion of an asymmetric molecule/particle can affect the meeting probabilities of this particle with targets located differently in relation to its initial orientation direction.

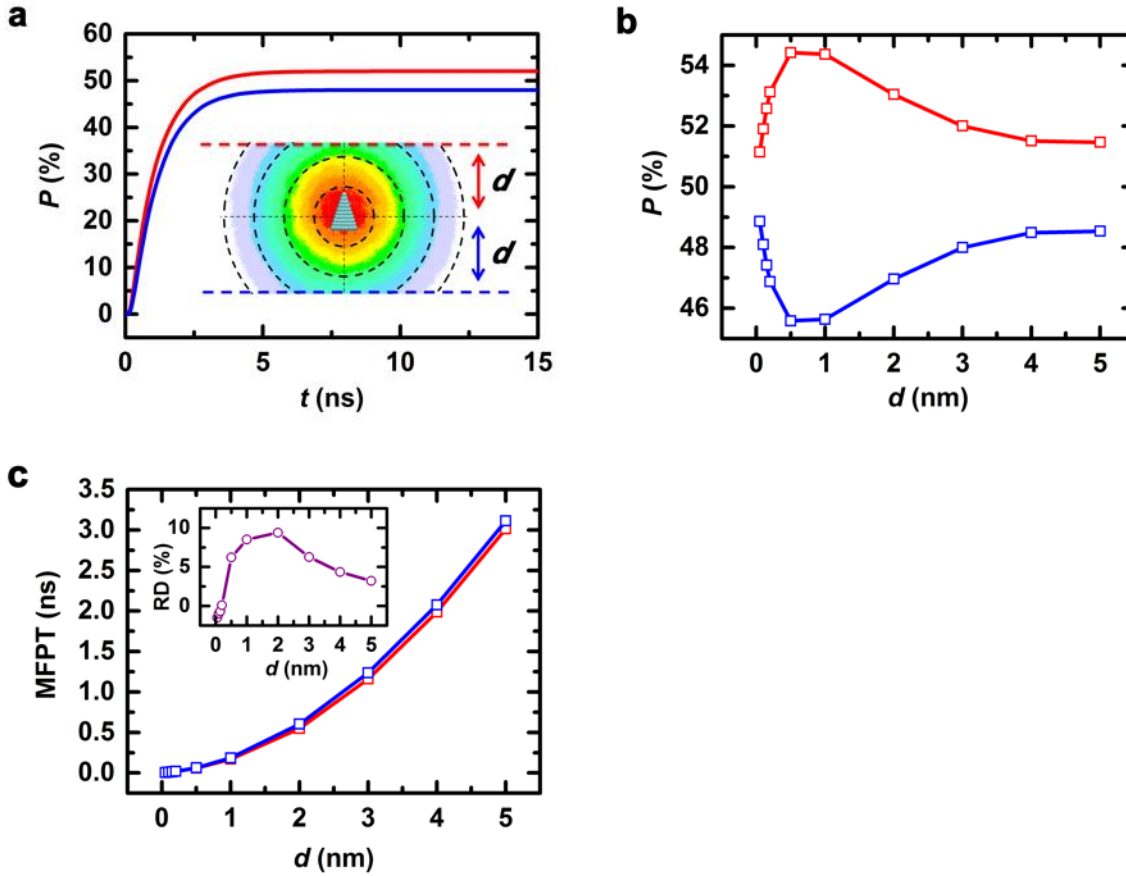


Figure 5. (a) Probability for a pyramid-shaped model particle of height  $h = 1.68$  nm to be absorbed by one of the two boundaries after time  $t$ . The planar absorbing boundaries are located at  $z = \pm 3$  nm, respectively. The inset shows the probability distribution function of the CoM position of the particle as a function of time. (b) Plateau values of the absorbed probabilities at the two boundaries with respect to the initial distance  $d$  from the CoM of the model particle to the boundaries. (c) Mean first passage times,  $\tau_f(z = \pm d)$ , for the model particles to reach the two absorbing boundaries. The inset shows the relative difference (RD) in  $\tau_f(z = \pm d)$  as calculated by  $[\tau_f(z = d) - \tau_f(z = -d)]/[P(z = d)\tau_f(z = d) + P(z = -d)\tau_f(z = -d)]$ .

The example system is set up as for a typical first passage time (FPT) problem. A pyramid-shaped particle of height  $h = 1.68$  nm is introduced into the solvent of small LJ particles with its center of mass located at the origin of the Cartesian coordinate frame and its principal orientation aligned along the positive  $z$ -direction, as sketched in Fig. 1(b). Two planar absorbing boundaries are placed in parallel to the  $x$ - $y$  plane and located at  $z = d$  and  $-d$ , respectively, see the inset in Fig. 5(a). The

particle is released at time  $t = 0$  to allow for free diffusion. When the CoM of the particle reaches any one of the two absorbing boundaries for the first time, it is considered to be absorbed and the corresponding simulation time, namely the first passage time, is recorded. This procedure is repeated many times until sufficient statistics is achieved. Simulation results in Fig. 5(a) show clearly that the directional drift of the model particle has led to a higher probability for it to be absorbed by the boundary located at  $z = d$ , *i. e.*, pointed to by its original orientation. The plateau values of the absorbed probabilities of the particles by the two boundaries differ by about 4% for  $d = \pm 3$  nm. It is noted that for model particles of this size the maximum drift value is only  $A \approx 0.15$  nm (see Fig. 4), which is much smaller than the initial distance  $d$  of the particle CoM to the boundaries. As shown in Fig. 5(b), the difference in the absorbed probabilities reaches a peak value in between  $d = 0.5$  to 1 nm, then gradually decreases with the increase of  $d$ , but still doesn't vanish after  $d = 5$  nm ( $> h = 1.68\text{nm} \gg A$ ). The simulation data on the mean first passage times [Fig. 3(c)],  $\tau_f(z = \pm d)$ , also show the long-term effect of the directional drift. The difference in  $\tau_f(z = d)$  and  $\tau_f(z = -d)$  is about 75 ps for  $d = 3$  nm and 98 ps for  $d = 5$  nm, which account for more than 6% and 3% of the averaged mean FPT ( $P(z = d)\tau_f(z = d) + P(z = -d)\tau_f(z = -d) = 1.2$  ns and 3.0 ns), respectively. As implied in Fig. 3 and Eq. (21), the drifting effect can be amplified by using particles of larger sizes or of different asymmetric shapes. It is thus possible to detect this process in experiments by employing well-selected asymmetric particles/molecules with embedded magnetic or electric dipole moments and applying external field to achieve the initial particle orientation.

On the other hand, the diffusion-reaction problems are encountered in many biological, chemical and physical processes, such as gene delivery and viral infection which involve the kinetically limited search processes for nuclear sites by nucleic acids.<sup>59-62</sup> The intracellular signaling between macromolecules or organelle in cell is also carried out by small signal molecules approaching the receptors within several nanometers where the meeting probability is the key.<sup>63-66</sup> Since all of the involved molecules are of asymmetric shapes, to determine the role of directional drift in the dynamics of these processes remains to be an open and challenging research subject.

Another interesting topic would be the design of novel bio-sensors by taking advantage of the biased meeting probabilities of the asymmetric particles in relation to their initial orientation as shown in Fig.5.

## Conclusion

We have shown using molecular dynamics simulations that solute molecules/particles with broken central symmetry in dilute solutions undergo a time-dependent directional motion process along their original orientation directions. Although in conventional theories particle drifting can only happen in the presence of external situational factors, such as concentration or temperature gradient, our simulation results reveal that for asymmetric particles the directional motion is intrinsic and so takes place even without any external interference. The physical origin of the effective driving force for the directional motion can be attributed to the imbalanced fluctuating forces acting on the particles by surrounding solvent molecules during the particle rotational relaxation. Our theoretical analysis predicts a linear relationship between the mean displacement and the autocorrelation function of the particle orientation,  $\langle z(t) \rangle \approx A[1-C_\phi(t)]$ , [Eq. (17)], owing to the coupling between the translational and rotational motion of the particle, which is validated by our MD simulations. As a result, the drift or mean displacement gets saturated after a sufficiently long time at which the autocorrelation function of the particle orientation decays to zero. The impact of the drift may be more significant for large asymmetric particles (e.g., colloidal particles) in the sense of absolute magnitude, since the saturated value of the drift grows with the size of the particles. This indicates at micrometer scale, there should be remarkable directional drift that can be directly observed when we consider the initial orientation of the asymmetrical particle. However, at micrometer (and may even macroscopic) scale, there lacks a proper theoretical description for the thermal noise since the system is too big for all-atom MD and the Langevin equation introduces an statistical (maybe artificial) random noise. Therefore, we are working towards a numerical scheme for those systems. We note that the noise induced nonlinear translation-rotation coupling has not been considered in

the present theory of the Brownian motion of the particle with low symmetry, so that the directional drift cannot be obtained theoretically. We think a wide range of studies and applications, both theoretically and experimentally, will be evoked by considering the initial orientation of molecules/particles.

In this paper, we only consider the directional drift along one direction (initial particle orientation), while the non-zero drift can actually occur in any direction for particles or molecules with broken central geometric symmetry within a finite time. Moreover, other types of asymmetries, such as the inhomogeneous mass distribution, charge distribution, hydrophobic/hydrophilic domains, will also induce the drifting behavior, which will be discussed in later works.

A further remark we would like to make is that the observed directional drift will not lead to a perpetual mobile that violates the second law of thermodynamics. As shown above, the drift behavior of asymmetric particles only take place in the directions along their initial orientations. In equilibrium systems, the orientations of the particles have equal probability in all directions. After averaging over all possible initial orientations of the particles, the mean displacements are zero at any time and so there is no directional drift in the system, which is consistent with the statistical mechanics principles. In the SI, we have demonstrated that one cannot extract mechanical energy from a thermal bath by restraining the orientations of the particles. To make use of the directional drift phenomenon, external energy input is required.

The finding of the intrinsic directional motion process of asymmetric particles may be directly relevant to many physical, chemical and biological processes and their practical applications, such as the diffusion-reaction processes of biomolecules in living cells and nanoparticles in various nano-systems that usually happen within finite timescales. Our simulation results should also be of strong interests for the study of statistical mechanics, because they reveal a pre-diffusive process,

which is beyond the traditional theory of Einstein diffusion relationship, and so call for new theoretical models. Our work indicates that there always exist nonequilibrium processes in equilibrium state and so there exists a limit for splitting an equilibrium system. In other words, the behavior of a single molecule/several molecules in an equilibrium system may exceed the limit of the laws of thermodynamics. The physical picture of the equilibrium state is actually chaos instead of random and the equilibrium system consists of various nonequilibrium processes like the motion of asymmetrical molecule. This also suggests that theoretical description of the equilibrium state of systems consisting of asymmetric molecules must be divided into different time and length regimes to take into account the transitions from initial ballistic motion, to short-time and nano-scale directional motion, and then to long-time isotropic Brownian-like diffusion.

### **Simulation Method**

The model particles we simulated were shaped as triangular pyramids, as shown in Fig. 1(a), where three side surfaces were identical isosceles triangles with the angle of  $36^\circ$  and the bottom surfaces were regular triangles. Five model particles of different sizes were built by bonding Leonard-Jones (LJ) particles to give the particle height  $h = 0.19$  nm, 0.37 nm, 0.56 nm, 1.12 nm, 1.68 nm [Fig. 1(a)], which contained 4, 10, 20, 84, 220 LJ particles, respectively. We put every model particle in a cubic box of dimensions  $4$  nm  $\times$   $4$  nm  $\times$   $4$  nm with periodic boundary conditions (except that  $12$  nm  $\times$   $12$  nm  $\times$   $12$  nm for particles with  $h = 1.12$  nm and  $18$  nm  $\times$   $18$  nm  $\times$   $18$  nm for particles with  $h = 1.68$  nm) filled with LJ particles as solvent at the same concentration of  $17$  nm<sup>-3</sup>. In SI8.1 we demonstrated that the finite size effects are negligible for the simulation results on the directional motion of the model particles. All LJ particles had the same mass of  $m_{LJ}=12.011$  u and the same force field parameters ( $\sigma = 0.375$  nm,  $\varepsilon = 0.439$  kJ mol<sup>-1</sup>). The cut-off distance for van de Waals (vdW) interactions was set to 1.3 nm. There was no Coulomb interaction in this system. The temperature was maintained at 300 K by velocity-rescale thermostat<sup>67</sup>. A time step of 2 fs was used, and the neighbor list was updated every 10 steps. Using Gromacs 4.6<sup>68</sup> software, we performed 5 independent simulation runs for each system

containing a given model particle immersed in solvents, starting from different initial configurations. Each system was first equilibrated for 20 ns and then ran for another 200 ns for analysis. The calculation of the PDFs of the CoMs and consequently the mean displaces of the model particles were carried out by taking time origins separated by 1ps along the MD trajectory. Thus we had about 1 million samples of each model particle for statistical analysis.

\* Corresponding author. Email: fanghaiping@sinap.ac.cn

† Corresponding author. Email: zuwei.wang@reading.ac.uk

## References

- 1 Ball, P. Water as an active constituent in cell biology. *Chem. Rev.* **108**, 74-108 (2008).
- 2 de Groot, B. L. & Grubmuller, H. Water permeation across biological membranes: Mechanism and dynamics of aquaporin-1 and GlpF. *Science* **294**, 2353-2357 (2001).
- 3 von Hansen, Y., Gekle, S. & Netz, R. R. Anomalous anisotropic diffusion dynamics of hydration water at lipid membranes. *Phys. Rev. Lett.* **111**, 118103 (2013).
- 4 Echeverria, I., Makarov, D. E. & Papoian, G. A. Concerted dihedral rotations give rise to internal friction in unfolded proteins. *J. Am. Chem. Soc.* **136**, 8708-8713 (2014).
- 5 Di Rienzo, C., Piazza, V., Gratton, E., Beltram, F. & Cardarelli, F. Probing short-range protein Brownian motion in the cytoplasm of living cells. *Nat. Commun.* **5**, 5891 (2014).
- 6 Ahmad, M., Gu, W. & Helms, V. Mechanism of fast peptide recognition by SH3 domains. *Angew. Chem. Int. Edit.* **47**, 7626-7630 (2008).
- 7 Schiessel, H., Widom, J., Bruinsma, R. F. & Gelbart, W. M. Polymer reptation and nucleosome repositioning. *Phys. Rev. Lett.* **86**, 4414-4417 (2001).
- 8 Robertson, R. M., Laib, S. & Smith, D. E. Diffusion of isolated DNA molecules: Dependence on length and topology. *Proc. Natl. Acad. Sci. U. S. A.* **103**, 7310-7314 (2006).
- 9 Phillips, R., Kondev, J. & Theriot, J. *Physical Biology of the Cell.* (Garland Science, 2008).
- 10 Dixit, S., Crain, J., Poon, W. C. K., Finney, J. L. & Soper, A. K. Molecular segregation observed in a concentrated alcohol-water solution. *Nature* **416**, 829-832 (2002).
- 11 Zhang, R. L., Xu, Y. S., Wen, B. H., Sheng, N. & Fang, H. P. Enhanced permeation of a hydrophobic fluid through particles with hydrophobic and hydrophilic patterned surfaces. *Sci. Rep.* **4**, 5738 (2014).
- 12 Bahng, J. H. *et al.* Anomalous dispersions of 'hedgehog' particles. *Nature* **517**, 596-599, (2015).
- 13 Zhao, L. *et al.* Reversible state transition in nanoconfined aqueous solutions. *Phys. Rev. Lett.* **112**, 078301 (2014).
- 14 de Sancho, D., Sirur, A. & Best, R. B. Molecular origins of internal friction effects on protein-folding rates. *Nat. Commun.* **5**, 4307 (2014).
- 15 Zhang, M., Zuo, G. H., Chen, J. X., Gao, Y. & Fang, H. P. Aggregated gas molecules: Toxic to protein? *Sci. Rep.* **3**, 1660 (2013).
- 16 Demichelis, R., Raiteri, P., Gale, J. D., Quigley, D. & Gebauer, D. Stable prenucleation mineral clusters are liquid-like ionic polymers. *Nat. Commun.* **2**, 590 (2011).
- 17 Wang, Z. W. & Larson, R. G. Molecular dynamics simulations of threadlike

- cetyltrimethylammonium chloride micelles: Effects of sodium chloride and sodium salicylate salts. *J. Phys. Chem. B* **113**, 13697-13710 (2009).
- 18 Liang, Y., Ozawa, M. & Krueger, A. A general procedure to functionalize agglomerating nanoparticles demonstrated on nanodiamond. *ACS Nano* **3**, 2288-2296 (2009).
- 19 Herves, P. *et al.* Catalysis by metallic nanoparticles in aqueous solution: model reactions. *Chem. Soc. Rev.* **41**, 5577-5587 (2012).
- 20 Einstein, A. *Investigations on the Theory of the Brownian Movement.* (Dover Publications, Inc., 1956).
- 21 Han, Y. *et al.* Brownian motion of an ellipsoid. *Science* **314**, 626-630 (2006).
- 22 Brenner, H. Coupling between translational and rotational Brownian motions of rigid particles of arbitrary shape: I. Helicoidally isotropic particles. *J. Colloid Sci.* **20**, 104-122 (1965).
- 23 Brenner, H. Coupling between translational and rotational Brownian motions of rigid particles of arbitrary shape: II. General theory. *J. Colloid Interface Sci.* **23**, 407-436 (1967).
- 24 Wegener, W. A. Diffusion-coefficients for rigid macromolecules with irregular shapes that allow rotational-translational coupling. *Biopolymers* **20**, 303-326 (1981).
- 25 Harvey, S. C. & Garcia De La Torre, J. Coordinate systems for modeling the hydrodynamic resistance and diffusion-coefficients of irregularly shaped rigid macromolecules. *Macromolecules* **13**, 960-964 (1980).
- 26 Sheng, N., Tu, Y. S., Guo, P., Wan, R. Z. & Fang, H. P. Asymmetrical free diffusion with orientation-dependence of molecules in finite timescales. *Sci. China-Phys. Mech. Astron.* **56**, 1047-1052 (2013).
- 27 Sheng, N., Tu, Y. S., Guo, P., Wan, R. Z. & Fang, H. P. Diffusion of an ammonia molecule in water in a very short time period. *J. Hydrodyn.* **24**, 969-970 (2012).
- 28 Chakrabarty, A. *et al.* Brownian motion of boomerang colloidal particles. *Phys. Rev. Lett.* **111**, 160603 (2013).
- 29 Chakrabarty, A. *et al.* Brownian motion of arbitrarily shaped particles in two dimensions. *Langmuir* **30**, 13844-13853 (2014).
- 30 Franosch, T. *et al.* Resonances arising from hydrodynamic memory in Brownian motion. *Nature* **478**, 85-88 (2011).
- 31 Huang, R. X. *et al.* Direct observation of the full transition from ballistic to diffusive Brownian motion in a liquid. *Nat. Phys.* **7**, 576-580 (2011).
- 32 Pusey, P. N. Brownian motion goes ballistic. *Science* **332**, 802-803 (2011).
- 33 Song, B. *et al.* Irreversible denaturation of proteins through aluminum-induced formation of backbone ring structures. *Angew. Chem. Int. Edit.* **53**, 6357-6363 (2014).
- 34 Tu, Y. S. *et al.* Destructive extraction of phospholipids from Escherichia coli membranes by graphene nanosheets. *Nat. Nanotechnol.* **8**, 594-601 (2013).
- 35 Hubbell, W. L., Cafiso, D. S. & Altenbach, C. Identifying conformational changes with site-directed spin labeling. *Nat. Struct. Biol.* **7**, 735-739 (2000).
- 36 Yang, H. *et al.* Protein conformational dynamics probed by single-molecule electron transfer. *Science* **302**, 262-266 (2003).
- 37 Striemer, C. C., Gaborski, T. R., McGrath, J. L. & Fauchet, P. M. Charge- and size-based separation of macromolecules using ultrathin silicon membranes. *Nature* **445**, 749-753 (2007).
- 38 Squires, T. M., Messinger, R. J. & Manalis, S. R. Making it stick: convection, reaction and diffusion in surface-based biosensors. *Nat. Biotechnol.* **26**, 417-426 (2008).
- 39 Hatch, A. *et al.* A rapid diffusion immunoassay in a T-sensor. *Nat. Biotechnol.* **19**, 461-465 (2001).
- 40 Song, B., Cuniberti, G., Sanvito, S. & Fang, H. P. Nucleobase adsorbed at graphene devices: Enhance bio-sensorics. *Appl. Phys. Lett.* **100**, 063101 (2012).
- 41 Tsapis, N., Bennett, D., Jackson, B., Weitz, D. A. & Edwards, D. A. Trojan particles: Large porous carriers of nanoparticles for drug delivery. *Proc. Natl. Acad. Sci. U. S. A.* **99**, 12001-12005 (2002).

- 42 Dittrich, P. S. & Manz, A. Lab-on-a-chip: microfluidics in drug discovery. *Nat. Rev. Drug Discov.* **5**, 210-218 (2006).
- 43 Hummer, G., Rasaiah, J. C. & Noworyta, J. P. Water conduction through the hydrophobic channel of a carbon nanotube. *Nature* **414**, 188-190 (2001).
- 44 Tu, Y. S. *et al.* Water-mediated signal multiplication with Y-shaped carbon nanotubes. *Proc. Natl. Acad. Sci. U. S. A.* **106**, 18120-18124 (2009).
- 45 Falk, K., Sedlmeier, F., Joly, L., Netz, R. R. & Bocquet, L. Molecular origin of fast water transport in carbon nanotube membranes: Superlubricity versus curvature dependent friction. *Nano Lett.* **10**, 4067-4073 (2010).
- 46 Zhu, F. Q., Tajkhorshid, E. & Schulten, K. Collective diffusion model for water permeation through microscopic channels. *Phys. Rev. Lett.* **93**, 224501 (2004).
- 47 Chandler, D. Interfaces and the driving force of hydrophobic assembly. *Nature* **437**, 640-647 (2005).
- 48 Michaelides, A. & Morgenstern, K. Ice nanoclusters at hydrophobic metal surfaces. *Nat. Mater.* **6**, 597-601 (2007).
- 49 Mazza, M. G., Giovambattista, N., Starr, F. W. & Stanley, H. E. Relation between rotational and translational dynamic heterogeneities in water. *Phys. Rev. Lett.* **96**, 057803 (2006).
- 50 Kang, S. G. *et al.* Hydrophobic Interaction Drives surface-assisted epitaxial assembly of amyloid-like peptides. *J. Am. Chem. Soc.* **135**, 3150-3157 (2013).
- 51 Koga, K., Gao, G. T., Tanaka, H. & Zeng, X. C. Formation of ordered ice nanotubes inside carbon nanotubes. *Nature* **412**, 802-805 (2001).
- 52 Mashl, R. J., Joseph, S., Aluru, N. R. & Jakobsson, E. Anomalous immobilized water: A new water phase induced by confinement in nanotubes. *Nano Lett.* **3**, 589-592 (2003).
- 53 Sint, K., Wang, B. & Kral, P. Selective Ion passage through functionalized graphene nanopores. *J. Am. Chem. Soc.* **130**, 16448-16449 (2008).
- 54 Yeh, I. C. & Hummer, G. System-size dependence of diffusion coefficients and viscosities from molecular dynamics simulations with periodic boundary conditions. *J. Phys. Chem. B.* **108**, 15873-15879 (2004).
- 55 van der Hoef, M. A., Frenkel, D. & Ladd, A. J. C. Self-diffusion of colloidal particles in a two-dimensional suspension: Are deviations from Fick's law experimentally observable? *Phys. Rev. Lett.* **67**, 3459-3462 (1991).
- 56 Zheng, Z. Y. & Han, Y. L. Self-diffusion in two-dimensional hard ellipsoid suspensions. *J. Chem. Phys.* **133**, 124509 (2010).
- 57 Doi, M. & Edwards, S. F. *The Theory of Polymer Dynamics.* (Oxford University Press, 1986).
- 58 Chandler, D. *Introduction to Modern Statistical Mechanics.* (Oxford University Press, 1987).
- 59 Guerin, T., Benichou, O. & Voituriez, R. Non-Markovian polymer reaction kinetics. *Nat. Chem.* **4**, 568-573 (2012).
- 60 Wong, S. Y., Pelet, J. M. & Putnam, D. Polymer systems for gene delivery-past, present, and future. *Prog. Polym. Sci.* **32**, 799-837 (2007).
- 61 Dinh, A. T., Pangarkar, C., Theofanous, T. & Mitragotri, S. Understanding intracellular transport processes pertinent to synthetic gene delivery via stochastic simulations and sensitivity analyses. *Biophys. J.* **92**, 831-846 (2007).
- 62 Dinh, A. T., Theofanous, T. & Mitragotri, S. A model for intracellular trafficking of adenoviral vectors. *Biophys. J.* **89**, 1574-1588 (2005).
- 63 Campbell, N. A. & Reece, J. B. *Biology.* (Benjamin Cummings, 2002)
- 64 Rodbell, M. Role of Hormone Receptors and Gtp-Regulatory Proteins in Membrane Transduction. *Nature* **284**, 17-22 (1980).
- 65 Gilman, A. G. A Protein Binding Assay for Adenosine 3'-5'-Cyclic Monophosphate. *P Natl Acad Sci USA* **67**, 305-& (1970).
- 66 Berridge, M. J. & Irvine, R. F. Inositol Phosphates and Cell Signaling. *Nature* **341**, 197-205

- (1989).
- 67 Bussi, G., Donadio, D. & Parrinello, M. Canonical sampling through velocity rescaling. *J. Chem. Phys.* **126**, 014101 (2007).
- 68 Hess, B., Kutzner, C., van der Spoel, D. & Lindahl, E. GROMACS 4: Algorithms for highly efficient, load-balanced, and scalable molecular simulation. *J. Chem. Theory Comput.* **4**, 435-447 (2008).

## Acknowledgements

We thank Prof. JI Qing and Prof. HU Jun for helpful discussions. Z. Wang also acknowledge Alexei Likhtman, Alex Lukyanov and Eugene Terentjev for valuable discussions. This work was supported by the National Natural Science Foundation of China (Grant Nos. 10825520, 11422542, 11175230 and 11290164), the Key Research Program of Chinese Academy of Sciences (Grant No. KJZD-EW-M03), the Deepcomp7000 and ScGrid of Supercomputing Center, the Computer Network Information Center of Chinese Academy of Sciences and the Shanghai Supercomputer Center of China.

## Author Contributions

H.F., Z.W. and N.S. contributed the idea and designed the project. N.S. performed the numerical simulations. H.F., Z.W. and N.S. carried out most of the theoretical analysis, and wrote the paper. Y.T., P.G. and R.W. performed some theoretical analysis. All authors discussed the results and commented on the manuscript.

## Additional information

**Supplementary Information** accompanies this paper on [www.nature.com/ncomms](http://www.nature.com/ncomms).

**Competing Financial Interests:** The authors declare that they have no competing financial interests.